

Residual thermal stresses in $\text{MoSi}_2\text{--Mo}_5\text{Si}_3$ in-situ composites

P. Peralta ^{a,*}, R. Dickerson ^a, J.R. Michael ^b, K.J. McClellan ^a, F. Chu ^a, T.E. Mitchell ^a

^a Los Alamos National Laboratory, Mail Stop K765, Los Alamos, NM 87545, USA

^b Sandia National Laboratory, Mail Stop 1405, Albuquerque, NM 87185, USA

Abstract

Residual thermal stresses in $\text{MoSi}_2\text{--Mo}_5\text{Si}_3$ in-situ composites are calculated for a dilute concentration of particles of one phase embedded in a matrix of the other, using the fields of anisotropic ellipsoidal inclusions. Additionally, the eutectic interfaces are modeled as boundaries between two anisotropic half-spaces. The misorientation between $\text{MoSi}_2\text{--Mo}_5\text{Si}_3$ is obtained from the literature for Mo_5Si_3 precipitates in MoSi_2 and by electron diffraction in the scanning electron microscope (SEM) for the opposite case. Tensile stresses of up to 3 GPa can develop after cooling from the eutectic temperature due to the thermal expansion mismatch between the phases. Electron microscopy of arc-melted Si-rich Mo_5Si_3 shows that stresses are relieved by intergranular fracture in Mo_5Si_3 and either dislocation plasticity or transgranular cracks in MoSi_2 , in a manner consistent with the calculations. © 1999 Elsevier Science S.A. All rights reserved.

Keywords: Residual thermal stress; Eutectic interfaces; Dislocation plasticity; Molybdenum disilicide; In-situ composites

1. Introduction

Molybdenum disilicide (MoSi_2) is a candidate material for structural applications at high temperatures [1]. However, its creep resistance is a major issue due to metal-like plasticity present above the brittle–ductile transition temperature (BDTT) [1]. Mo_5Si_3 has been considered a good reinforcement to improve the creep properties of MoSi_2 , due to its thermodynamic stability, good creep strength at high temperatures and eutectic reaction with MoSi_2 , from which in-situ composites can be obtained [2,3]. Mason and coworkers [2,3] have shown that directionally solidified $\text{MoSi}_2\text{--Mo}_5\text{Si}_3$ eutectics have better creep properties than other MoSi_2 -based composites. However, they reported the presence of cracks in their samples after processing them from the melt. These cracks are the likely result of residual stresses developed during cooling due to thermal expansion mismatch. Unusual cracking in MoSi_2 single crystals has been attributed to Mo_5Si_3 particles [4], and intergranular cracking in polycrystalline Mo_5Si_3 has been connected to thermal stresses at grain boundaries

[5]. Therefore, residual thermal stresses are calculated for a dilute concentration of particles of Mo_5Si_3 in a MoSi_2 matrix and vice versa, modeling the particles as anisotropic ellipsoidal inclusions. Additionally, eutectic interfaces are modeled as boundaries between two anisotropic half-spaces. Moreover, a Si-rich Mo_5Si_3 alloy was prepared to determine the microstructure and the orientation relationship (OR) of MoSi_2 particles embedded in Mo_5Si_3 . Transmission electron microscopy (TEM) and scanning electron microscopy (SEM) are used to study the failure modes due to the stresses.

2. Modeling

2.1. Anisotropic ellipsoidal inclusions and eutectic microstructure

The elastic fields of anisotropic ellipsoidal inclusions were obtained by Asaro and Bammert [6], who showed that there is a linear relationship between a stress free transformation strain ϵ_{ij}^t and the final strain ϵ_{ij}^c in the inclusion, i.e.:

$$\epsilon_{ij}^c = \mathbf{K}_{ijkl} \mathbf{C}_{klmn} \epsilon_{mn}^t \quad (1)$$

* Corresponding author.

where \mathbf{C} is the stiffness tensor of the matrix and \mathbf{K} is defined as follows [6]:

$$\mathbf{K}_{ipkj} = \frac{a_1 a_2 a_3}{8\pi} \int_0^\pi \int_0^{2\pi} \frac{\mathbf{z}_p \mathbf{z}_j \mathbf{M}_{ik}^{-1} + \mathbf{z}_i \mathbf{z}_j \mathbf{M}_{pk}^{-1}}{[(a_1 \mathbf{z}_1)^2 + (a_2 \mathbf{z}_2)^2 + (a_3 \mathbf{z}_3)^2]^{3/2}} d\theta d\phi \quad (2)$$

The a_i are the semi-axes of the ellipsoid, ϕ and θ are the azimuthal and polar angles in spherical coordinates and \mathbf{M} and \mathbf{z} are defined as [6]:

$$\mathbf{M}_{ik} = \mathbf{C}_{jikm} \mathbf{z}_j \mathbf{z}_m \quad (3)$$

$$\mathbf{z} = [\sin \phi \cos \theta, \sin \phi \sin \theta, \cos \phi]^T \quad (4)$$

If both ε_{ij}^t and ε_{ij}^c are known, the stress inside the inclusion equals:

$$\sigma_{ij}^{\text{inc}} = \mathbf{C}_{ijkm} (\varepsilon_{km}^c - \varepsilon_{km}^t) \quad (5)$$

and the stress immediately outside the inclusion can then be calculated as [7]:

$$\sigma_{ij}^{\text{mat}} = \mathbf{C}_{ijkl} (-\mathbf{C}_{pqmn} \varepsilon_{nm}^t \mathbf{N}_{kp}(\mathbf{n}) D^{-1}(\mathbf{n}) n_q n_l + \varepsilon_{kl}^t) + \sigma_{ij}^{\text{inc}} \quad (6)$$

where $\mathbf{N}(\mathbf{n})$ is the matrix of cofactors of the following tensor:

$$\mathbf{P}_{ik}(\mathbf{n}) = \mathbf{C}_{ijk} n_j n_l \quad (7)$$

\mathbf{n} is the normal to the surface of the ellipsoid and $D(\mathbf{n})$ is the determinant of $\mathbf{P}(\mathbf{n})$.

The transformation strain can be taken equal to the difference between the thermal expansion tensors of the two phases times the difference in temperature [8]:

$$\varepsilon_{ij}^t = (\alpha_{ij}^{\text{prec}} - \alpha_{ij}^{\text{mat}}) \Delta T \quad (8)$$

ΔT is taken as the difference between the eutectic temperature (1900°C [9]) and 25°C. Elastic and thermal properties were taken from [10] for MoSi_2 and from [5] for Mo_5Si_3 . They are shown in Table 1 and Table 2.

The integral in Eq. (2) was solved numerically using Gaussian integration with 16 quadrature points for each variable [11]. This produced results within 1% of analytical solutions shown in [12], for isotropic materials.

When the matrix and the inclusion do not have the same elastic constants it is necessary to find an equiva-

Table 1
Properties of monocrystalline MoSi_2 [10]

Elastic stiffness (GPa)	C_{11}	405
	C_{12}	117
	C_{13}	93
	C_{33}	508
	C_{44}	202
	C_{66}	194
Thermal expansion	α_{11}	8.2×10^{-6}
	α_{22}	8.2×10^{-6}
	α_{33}	9.4×10^{-6}

Table 2
Properties of monocrystalline Mo_5Si_3 [5]

Elastic stiffness (GPa)	C_{11}	446
	C_{12}	174
	C_{13}	140
	C_{33}	390
	C_{44}	110
	C_{66}	140
Thermal expansion	α_{11}	5.2×10^{-6}
	α_{22}	5.2×10^{-6}
	α_{33}	11.5×10^{-6}

lent transformation strain ε_{km}^* for an inclusion with the same properties as the matrix, such that the tractions at the interface between the matrix and the equivalent inclusion and the final constrained strain are the same as those in the real inclusion [12]. ε_{km}^* is found by using Eq. (1) with the following equation:

$$\sigma_{ij}^{\text{inc}} = \mathbf{C}_{ijkm}^{\text{inc}} (\varepsilon_{km}^c - \varepsilon_{km}^t) = \mathbf{C}_{ijkm}^{\text{mat}} (\varepsilon_{km}^c - \varepsilon_{km}^*) \quad (9)$$

The stresses for the eutectic are calculated using a model that can be applied to laminate composites [13], which is an approximation to the lamellar structure of the eutectic [2,3]. A system of equations is used to calculate the stresses, i.e.:

$$\begin{bmatrix} S_{1111}^{(+)} & S_{1122}^{(+)} & S_{1112}^{(+)} \\ S_{2211}^{(+)} & S_{2222}^{(+)} & S_{2212}^{(+)} \\ S_{1211}^{(+)} & S_{1222}^{(+)} & S_{1212}^{(+)} \end{bmatrix} \begin{bmatrix} \Delta\sigma_{11}^{(1)} \\ \Delta\sigma_{22}^{(1)} \\ \Delta\sigma_{12}^{(1)} \end{bmatrix} = \begin{bmatrix} \alpha_{11}^{(2)} - \alpha_{11}^{(1)} \\ \alpha_{22}^{(2)} - \alpha_{22}^{(1)} \\ \alpha_{12}^{(2)} - \alpha_{12}^{(1)} \end{bmatrix} \Delta T \quad (10)$$

where $S_{ijkl}^{(+)} = S_{ijkl}^{(2)} + S_{ijkl}^{(1)}$ are the sums of the compliances in both materials and $\Delta\sigma_{ij}^{(1)}$ is the ij ($ij = 11, 22, 12$) component of stress in material Eq. (1), with $\Delta\sigma_{ij}^{(2)} = -\Delta\sigma_{ij}^{(1)}$. The σ_{i3} components are assumed to be equal to zero. Further details are shown in [13].

2.2. Geometry and crystallography

The geometry and crystallography of Mo_5Si_3 precipitates in MoSi_2 was reported by Xiao and coworkers [14]. The precipitates were elongated parallelepipeds with the long axis along the $\langle 110 \rangle$ direction common to the two lattices and $(110)\text{MoSi}_2 \parallel (001)\text{Mo}_5\text{Si}_3$ and $(001)\text{MoSi}_2 \parallel (110)\text{Mo}_5\text{Si}_3$. Note from Table 1 and Table 2 that the thermal expansion mismatch is maximized for this misorientation, since the c axis of one material is aligned with one axis on the plane of transverse isotropy of the other; therefore, the thermal stresses are possibly the highest of all possible misorientations. The micrographs reported in [14], show that the Mo_5Si_3 precipitates can have different lengths and cross

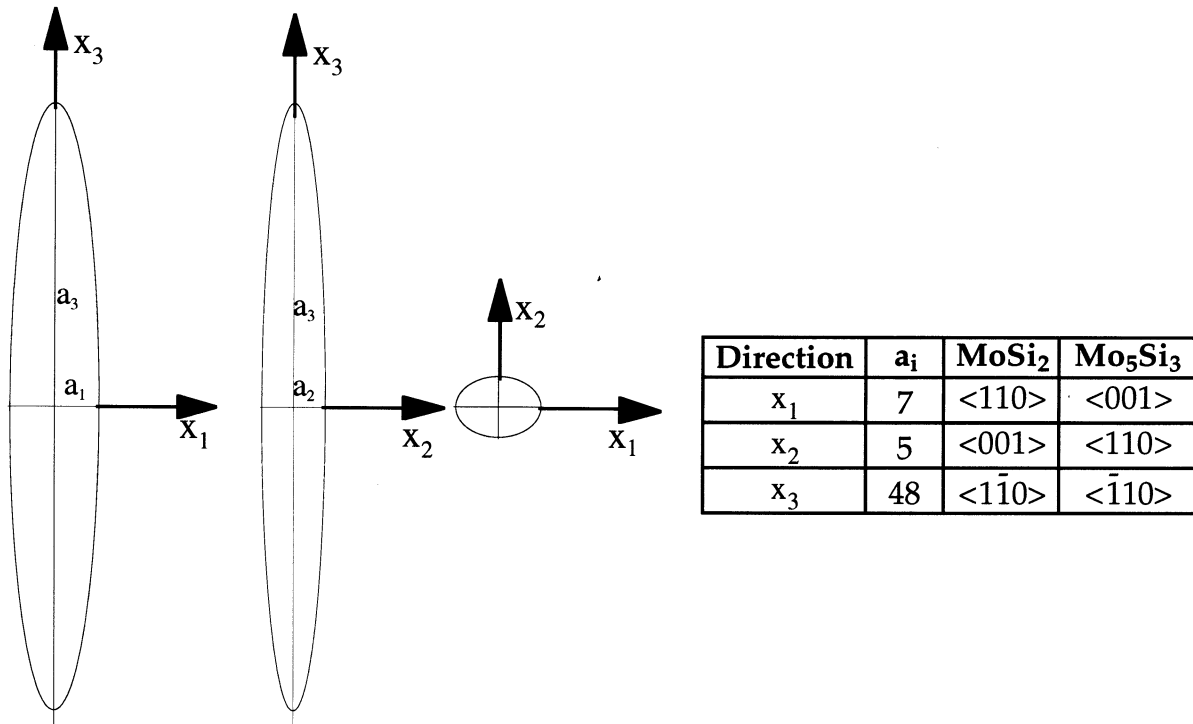


Fig. 1. Geometry and crystallography of ellipsoidal inclusions.

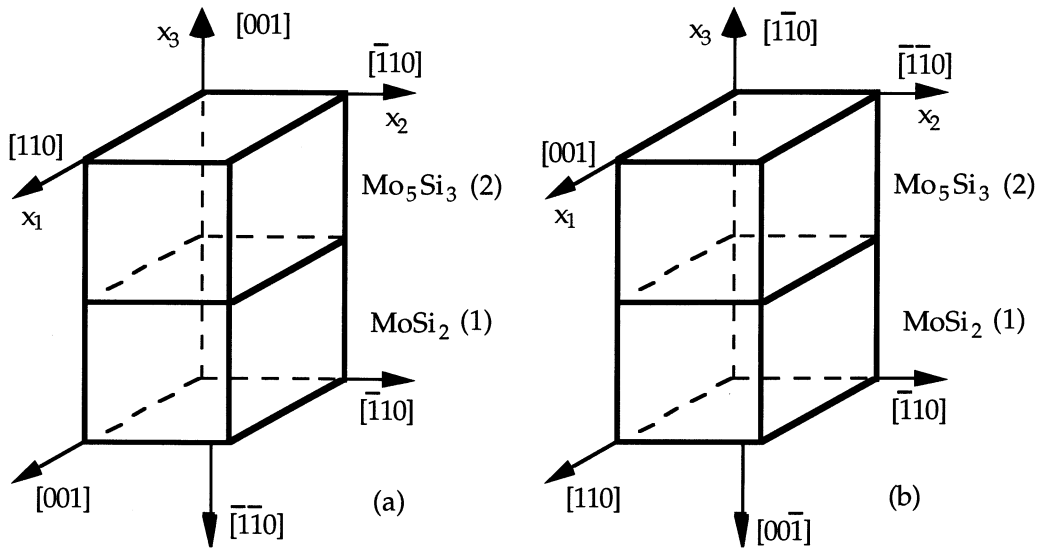


Fig. 2. Crystallography of eutectic interfaces. (a) First variant. (b) Second variant.

sections. Direct measurements showed that a typical aspect ratio between the three axes of the precipitates is 7:5:48. These proportions are therefore used to specify the geometry of the ellipsoidal inclusions, as shown in Fig. 1, as an approximation to the actual precipitates. However, the stresses obtained via the ellipsoidal inclusions should be a lower bound of those in the real precipitates, since their rectangular cross sections must produce higher stresses than the smooth curvature of an ellipsoid.

The same OR discussed above was found to be present in the eutectic microstructure [3]. Two configurations for the interfaces are reported in [3], $(110)\text{MoSi}_2 \parallel (001)\text{Mo}_5\text{Si}_3$ and $(001)\text{MoSi}_2 \parallel (110)\text{Mo}_5\text{Si}_3$, to within 15° . The complete crystallography used in the calculations is shown in Fig. 2.

Mason and Van Aken [2] reported TEM observations of small MoSi_2 precipitates in the Mo_5Si_3 phase of an Er containing eutectic. They found two ORs: one was the same as that of Mo_5Si_3 precipitates in MoSi_2

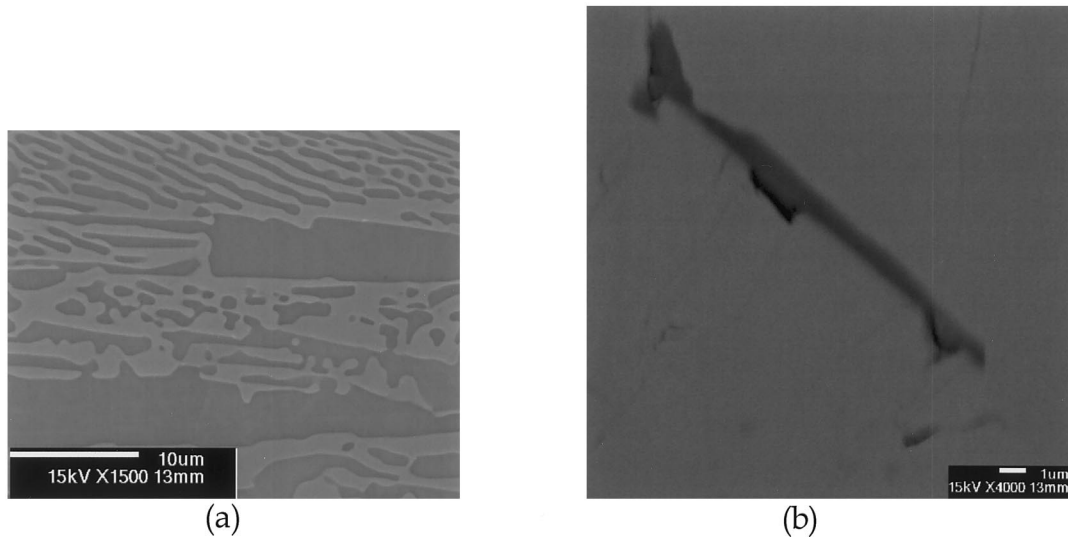


Fig. 3. Microstructure in Si-rich Mo_5Si_3 . (a) Eutectic. (b) Isolated MoSi_2 particle.

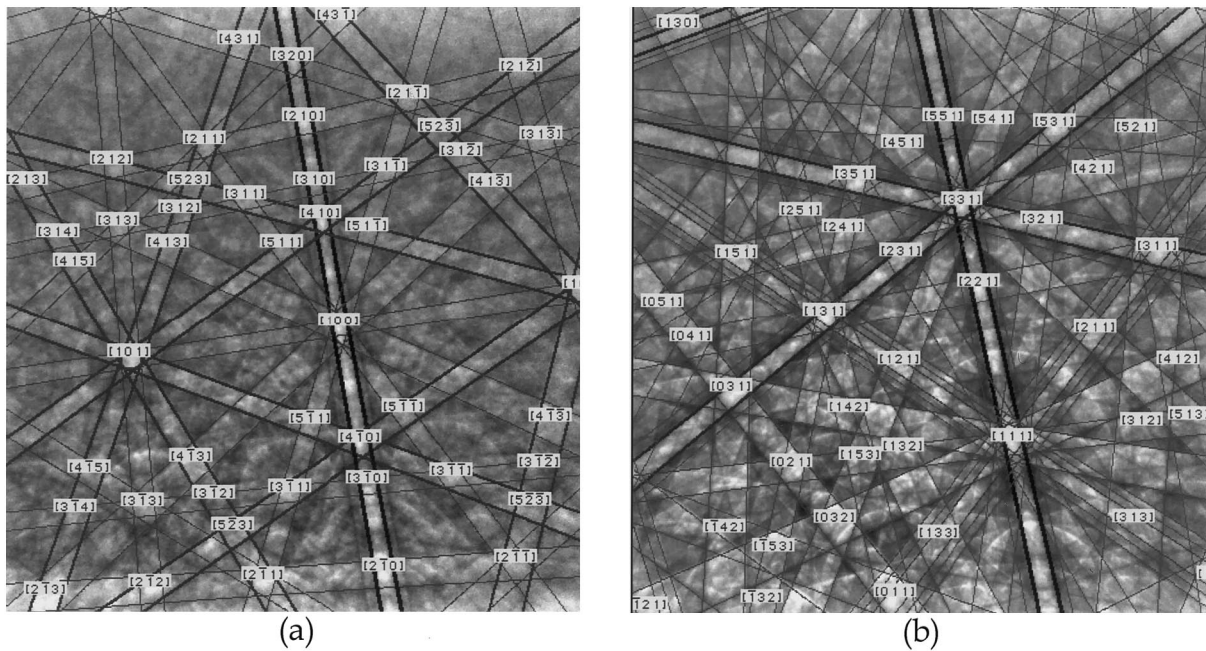


Fig. 4. Indexed EBS patterns for Si-rich Mo_5Si_3 . (a) Mo_5Si_3 matrix. (b) MoSi_2 particle.

and the other was $[111]\text{MoSi}_2\| [001]\text{Mo}_5\text{Si}_3$ and $(110)\text{MoSi}_2\| (330)\text{Mo}_5\text{Si}_3$, which was observed in growth perturbations of directionally solidified eutectics [3]. In order to verify if these misorientations, and the corresponding microstructures, are not affected by the presence of Er, Si-rich Mo_5Si_3 samples were prepared and examined. The experimental procedures used are described in the next section.

3. Experimental

Si-rich Mo_5Si_3 buttons with nominal composition $\text{Mo}_{57.6}\text{Si}_{42.4}$ were prepared from pure Mo and Si by arc

melting in Ar. Samples were cut from the buttons and polished with 600, 800 and 1200 grit SiC paper, and 1 μm diamond paste. These samples were examined in a JEOL 6300 FX SEM operating at 15 kV and equipped with a PGT X-ray detector to determine the microstructure and composition. This sample was used to obtain electron backscattering (EBS) Patterns of the Mo_5Si_3 matrix and the MoSi_2 particles by mounting the sample at a tilt of 70.5° in a JEOL 6400 SEM equipped with a LaB_6 electron source working at 20 kV with a beam current of about 5 nA. Patterns were recorded using the CCD-based detector described in [15], with exposure times of 5 s. The patterns were automatically indexed using software developed at Sandia National

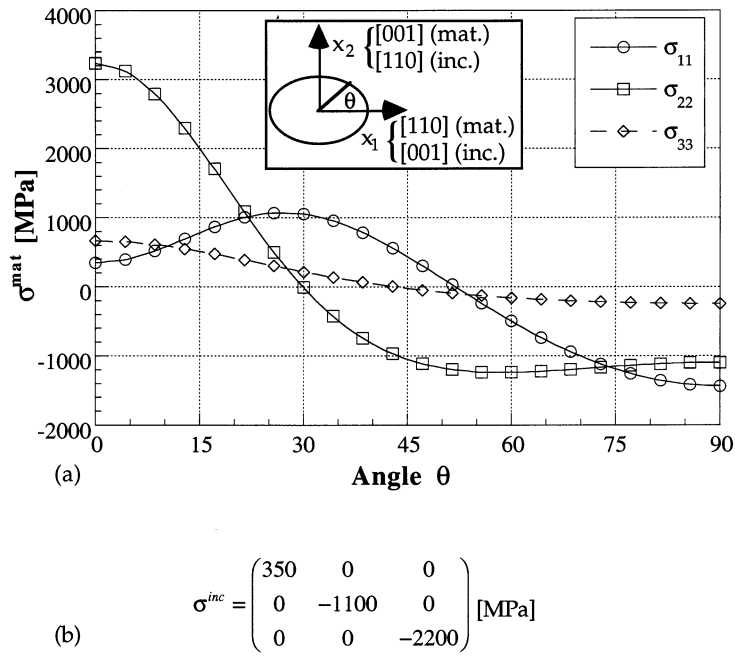


Fig. 5. Stresses for an ellipsoidal precipitate of Mo₅Si₃ embedded in a matrix of MoSi₂. (a) Matrix. (b) Precipitate.

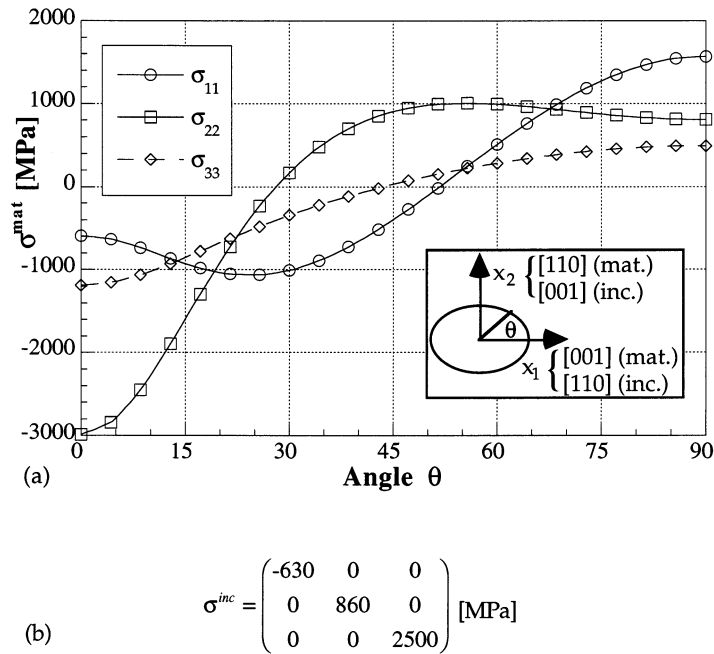


Fig. 6. Stresses for an ellipsoidal particle of MoSi₂ embedded in a matrix of Mo₅Si₃. (a) Matrix. (b) Precipitate.

Laboratories, which calculates an orientation matrix with respect to the microscope reference frame.

4. Results and discussion

4.1. Microstructure and orientation relationship in Si-rich Mo₅Si₃

The microstructure of the Si-rich Mo₅Si₃ after arc-

melting was not uniform, since it consisted of both layered eutectic (Fig. 3a), and isolated particles of MoSi₂ (Fig. 3b). Note that the MoSi₂ particle shows an elongated configuration, but the cross section is not as uniform as that of Mo₅Si₃ precipitates in MoSi₂. This is similar to observations of MoSi₂ precipitates in Er-doped Mo₅Si₃ [2]. The indexed EBS patterns obtained at and around a similar particle are shown in Fig. 4. The orientation matrices for the matrix and the precipitate are the following:

$$\sigma^{MoSi_2} = \begin{pmatrix} -985 & 0 & 0 \\ 0 & 925 & 0 \\ 0 & 0 & 0 \end{pmatrix} [\text{MPa}] \quad \sigma^{Mo_5Si_3} = \begin{pmatrix} 985 & 0 & 0 \\ 0 & -925 & 0 \\ 0 & 0 & 0 \end{pmatrix} [\text{MPa}] \quad (\text{a})$$

$$\sigma^{MoSi_2} = \begin{pmatrix} 2010 & 0 & 0 \\ 0 & 1590 & 0 \\ 0 & 0 & 0 \end{pmatrix} [\text{MPa}] \quad \sigma^{Mo_5Si_3} = \begin{pmatrix} -2010 & 0 & 0 \\ 0 & -1590 & 0 \\ 0 & 0 & 0 \end{pmatrix} [\text{MPa}] \quad (\text{b})$$

Fig. 7. Stresses for the eutectic microstructure. (a) First variant. (b) Second variant (as diagrammed in Fig. 2).

$$\mathbf{R}_{Mo_5Si_3} = \begin{bmatrix} 0.176 & -0.148 & -0.973 \\ -0.475 & 0.852 & -0.220 \\ 0.862 & 0.501 & 0.081 \end{bmatrix}$$

$$\mathbf{R}_{MoSi_2} = \begin{bmatrix} 0.703 & -0.651 & 0.285 \\ 0.384 & 0.011 & -0.923 \\ 0.598 & 0.759 & 0.258 \end{bmatrix} \quad (11)$$

and the rotation matrix between the two phases can then be calculated as follows:

$$\mathbf{R}_{mp} = \mathbf{R}_{MoSi_2}^{-1} \mathbf{R}_{Mo_5Si_3} \quad (12)$$

The real eigenvector of \mathbf{R}_{mp} is the axis common to both materials [16], in this case $[0.697, 0.717, -0.006]^T$. This is 0.9° away from $\langle 110 \rangle$. Similarly, the angle of rotation about this axis can also be obtained [16], and it equals 93.2° . A small deviation from the 90° angle has also been reported in Mo_5Si_3 precipitates in $MoSi_2$ [14], and in the eutectic [3]. This OR should result in high thermal stresses, as discussed before. Note also that the other OR reported for $MoSi_2$ and Mo_5Si_3 in both the eutectic and Er-doped Mo_5Si_3 [3], does not align the c and a axes of the two materials; therefore, the thermal expansion mismatch is not as high as that of the common misorientation. This and other misorientations were found during this study; however, given that the OR shown above should maximize the residual stresses, it will be used to carry out the stress analysis for all cases. In regard to the geometry of the particles, it will be assumed that it is the same as in Fig. 1, given that the $MoSi_2$ particles were also elongated and had the same OR with Mo_5Si_3 as that reported in [3,14], for Mo_5Si_3 in $MoSi_2$.

4.2. Residual stresses

4.2.1. Mo_5Si_3 particles in $MoSi_2$ and $MoSi_2$ particles in Mo_5Si_3

The stresses due to an Mo_5Si_3 precipitate in an $MoSi_2$ matrix are shown in Fig. 5, for a plane that contains the two small semi-axes of the inclusion (see insert in Fig. 5a). Note that the tensile stresses in the $MoSi_2$ matrix (Fig. 5a) reach a maximum of about 3.1 GPa (σ_{22}). This stress is also normal to the preferred cleavage plane in $MoSi_2$, i.e. (001) [4], making it likely to have cleavage

fracture in the matrix, unless another mechanism for stress relief is present. The stresses in the precipitate, (Fig. 5b), are high in compression for x_2 and x_3 and tensile only along x_1 . Note that the stress along the latter direction is quite low as compared with the stresses along the other two axes, suggesting that the Mo_5Si_3 precipitates are likely to stay free of cracks, even when there is little dislocation activity in the matrix, as was observed in the microstructure reported in [14]. The results of indentation testing on monocrystalline Mo_5Si_3 reported in [5] did not indicate a specific trend regarding the crystallography of possible cleavage planes in the material, so that no data are available at this time regarding cleavage strength or preferential cleavage planes.

The stresses due to an $MoSi_2$ precipitate in an Mo_5Si_3 matrix are shown in Fig. 6, for the same configuration as that used for the Mo_5Si_3 precipitates in the $MoSi_2$ matrix (insert in Fig. 6a). Note that the stresses in the matrix are approximately opposite to those shown in the previous section, as is expected since the role of each material has switched. The maximum tensile stress in the Mo_5Si_3 matrix is about 1.5 GPa along [001], and the second highest tensile stress is approximately 1 GPa along [110]. In the $MoSi_2$ particle, there is a high tensile stress, 2.5 GPa, along [110]. Note that the (110) plane is not one of preferred cleavage planes for $MoSi_2$, as discussed in [4], so fracture in a plane with a normal parallel to the long axis of the precipitate is unlikely in this case; however, there is a tensile stress of 860 MPa applied to the (001) plane, so that fracture on that plane is much more likely.

4.2.2. Eutectic microstructure

The stresses next to a planar interface in the lamellar eutectic microstructure after cooling from 1900°C are shown in Fig. 7. Note that for the first variant (Fig. 2a) the tensile stress in $MoSi_2$ is applied on a {110} plane, which is not a preferred cleavage plane [4]. The stresses for the second variant (Fig. 3b) are higher and tensile, with the highest stress (2 GPa) applied on a (001) plane, indicating that this variant is more likely to show cleavage fracture. The maximum stresses in either case are lower than those observed for the case of dilute concentration of particles; nevertheless, they are high

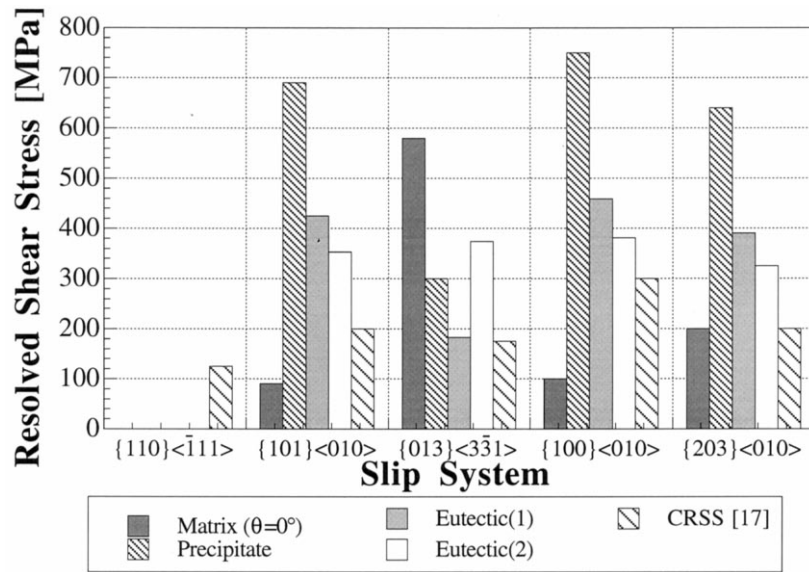


Fig. 8. RSS in MoSi₂ at 1000°C for all the cases studied.

enough that some dislocation activity should be present at least in MoSi₂. This will be discussed in the next section.

4.3. Dislocation activity

It is likely that at temperatures above the BDTT, $\approx 1000^\circ\text{C}$ [17], the stresses in MoSi₂ for the three cases studied are high enough to activate one or several slip systems. Taking into account that the equations are linear in ΔT , the stresses produced by cooling down to 1000°C from the eutectic temperature (1900°C) should

be smaller than those obtained at room temperature by a factor of $\Delta T_2/\Delta T_1 = 900/1875 = 0.48$. Therefore, the stress tensors for (a) the MoSi₂ matrix for $\theta = 0^\circ$ (where σ_{22} is maximum); (b) the MoSi₂ particles, and (c) the MoSi₂ in the two variants of the eutectic can be obtained at 1000°C. The resolved shear stresses (RSSs) can then be calculated for all slip systems and compared with the critical RSSs (CRSSs) at the same temperature. The results are presented in Fig. 8.

Note that, in most cases, the RSSs are higher than the corresponding CRSSs, indicating that extensive dislocation activity should be present in the MoSi₂ phase as the temperature decreases to the BDTT. According

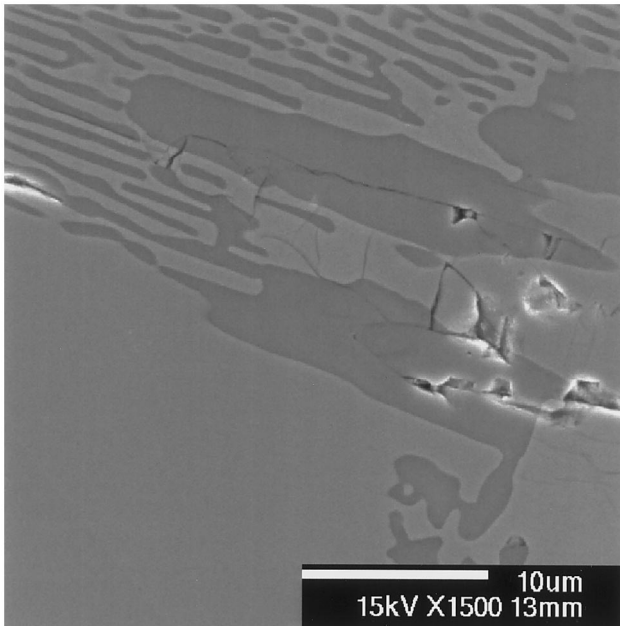


Fig. 9. Transgranular cracks in MoSi₂ particles (SEM).

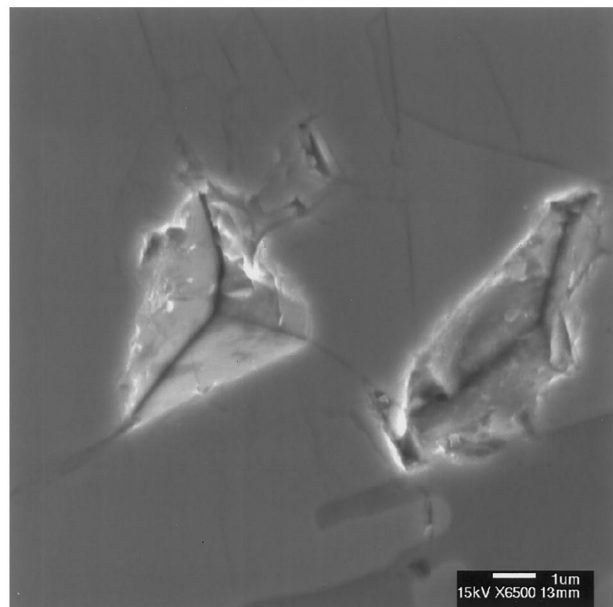


Fig. 10. Intergranular cracking in Mo₅Si₃ (SEM).

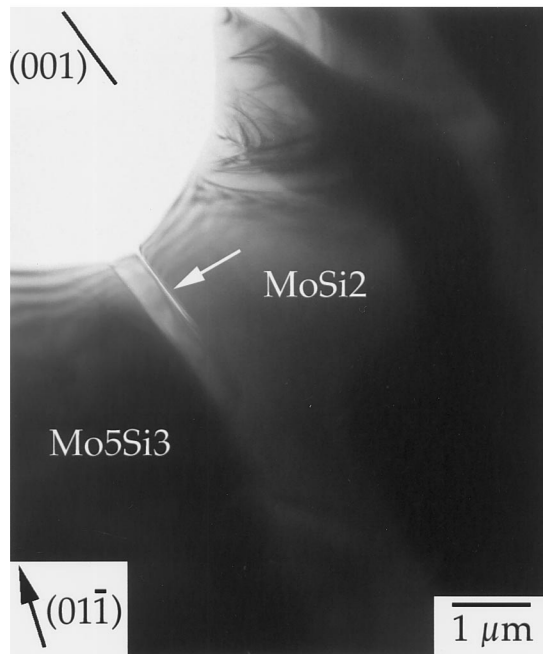


Fig. 11. TEM micrograph of a transgranular crack in MoSi_2 .

to Fig. 8, the highest dislocation activity should be in the isolated MoSi_2 particles, whereas the lowest activity should be in the MoSi_2 matrix, with the two eutectic variants somewhere in between. Note that the RSSs for the matrix are calculated at just one point, $\theta = 0^\circ$, and a different result can be obtained at another position, e.g. at $\theta = 90^\circ$ the RSSs of three slip systems are equal or higher than their CRSSs at 1000°C . Extensive dislocation activity must then be present around the precipitate, relieving the thermal stresses considerably, provided that the material spends enough time at a temperature above the BDTT to fully develop a plastic zone around the precipitates.

Regarding dislocation plasticity in Mo_5Si_3 , overall creep properties have been reported for single crystals [2], but no measurements of the CRSSs for the slip systems seem to be available in the open literature; therefore, it is not possible to make predictions regarding its dislocation activity in any of the microstructures.

4.4. Stress relief

4.4.1. SEM observations

Examination of the Si-rich Mo_5Si_3 material in the SEM showed that there were two main fracture modes in the material. The first was transgranular fracture in the MoSi_2 particles, as can be seen in Fig. 9. Note that the cracks are long and straight, suggesting that they are crystallographic in nature, and their trace is parallel to the long axis the precipitate, which agrees with the discussion offered in Section 4.2.1. This also suggests that dislocation activity inside these precipitates, if

present, is not enough to prevent brittle fracture in all cases. The rapid cooling derived from the arc-melting process could be one reason for insufficient plasticity inside the MoSi_2 precipitates. Note that there are some cracks in the matrix, probably transgranular, associated with the cracks in the precipitates. The second fracture mode was intergranular fracture in the Mo_5Si_3 matrix, as shown in Fig. 10. There are cracks along the boundaries inside the hole left behind by one grain, and careful observation shows that they extend beyond the hole into the bulk of the matrix, following the original grain boundaries, as is expected, according to [5].

4.4.2. TEM observations

Transgranular fracture of the MoSi_2 particles was observed in TEM as well (Fig. 11). The crystallography also shows that the crack trace is parallel to the trace of (001) in the plane of the foil, which is consistent with the presence of high tensile stresses on (001), according to the results of Section 4.2.2. Indications that dislocation plasticity can indeed relieve the thermal stresses to the point of avoiding cracking are shown in Fig. 12, where it can be seen that a dislocation network in the MoSi_2 matrix developed around an Mo_5Si_3 precipitate, without evidence of fracture at either phase or the interface between them. This suggests that proper heat treatment of MoSi_2 when Mo_5Si_3 precipitates are present could prevent cracking due to thermal stresses by allowing dislocations to relieve the stresses as temperature comes down. Note that dislocations are not readily visible in the MoSi_2 phase that did not have Mo_5Si_3 precipitates (Fig. 11), which could be due to rapid cooling, as

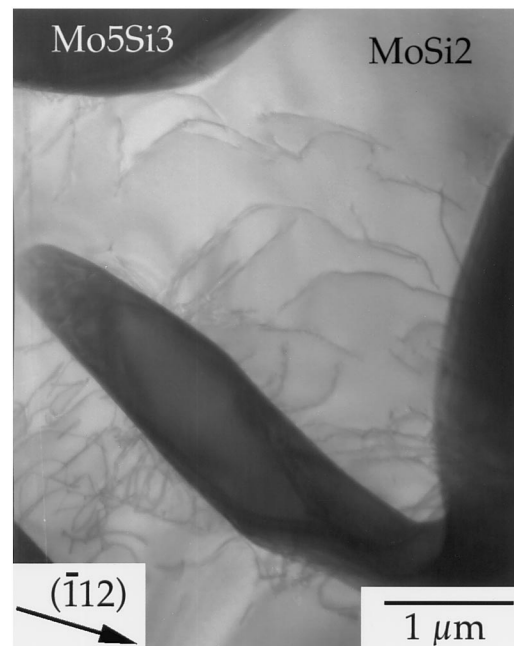


Fig. 12. TEM micrograph of a dislocation network in MoSi_2 with an embedded Mo_5Si_3 particle.

discussed above. This also suggests that composites with Mo_5Si_3 as the matrix and MoSi_2 as the ‘ductile phase’ could suffer from more cracking due to residual stresses than composites with an MoSi_2 matrix. The low number of slip systems in Mo_5Si_3 [2], and its low ductility at room temperature [5], make it difficult to relieve the thermal stresses via plastic deformation.

5. Summary

Composites of MoSi_2 – Mo_5Si_3 with dilute concentration of precipitates develop high residual stresses upon cooling from the eutectic temperature, with high tensile stresses in the preferred cleavage plane of MoSi_2 .

Stress relief in Si-rich Mo_5Si_3 occurs mostly through intergranular fracture in the Mo_5Si_3 matrix, and either transgranular fracture in MoSi_2 on the (001) plane, which is under high tensile stresses, or dislocation plasticity. The latter mechanism seemed more effective when an Mo_5Si_3 particle is completely surrounded by MoSi_2 .

The elastic analyses agree well with the observed failure modes, as they predicted both dislocation activity and transgranular fracture in MoSi_2 .

MoSi_2 – Mo_5Si_3 in-situ composites require heat treatment in order to relieve thermal stresses. This is likely to be more effective for an MoSi_2 matrix, given that its dislocation activity is higher at elevated temperatures than that of Mo_5Si_3 .

Acknowledgements

This work was supported by the US Department of

Energy, Office of Basic Energy Science, and a Director Funded Postdoctoral Fellowship at LANL (P. Peralta).

References

- [1] J.J. Petrovic, *Mat. Sci. Eng.* A193 (1995) 31–37.
- [2] D.P. Mason, D.C. Van Aken, *Acta Metall. Mater.* 43 (1995) 1201–1210.
- [3] D.P. Mason, D.C. Van Aken, J.F. Mansfield, *Acta Metall. Mater.* 43 (1995) 1189–1199.
- [4] P. Peralta, S.A. Maloy, F. Chu, J.J. Petrovic, T.E. Mitchell, *Scripta Mater.* 37 (1997) 1599–1604.
- [5] F. Chu, D.J. Thoma, K. McClellan, P. Peralta, *Synthesis and Properties of Mo_5Si_3 Single Crystals*, in these proceedings, 1998.
- [6] R.J. Asaro, D.M. Barnett, *J. Mech. Phys. Solids* 23 (1975) 77–83.
- [7] T. Mura, *Micromechanics of Defects in Solids*, 2nd, Kluwer, Boston, 1991.
- [8] M.-J. Pan, D.J. Green, J.R. Hellmann, *Scripta Mater.* 36 (1997) 1095–1100.
- [9] American Society for Metals, In: H. Baker (Ed.), *ASM Handbook, Volume 3: Alloy Phase Diagrams*, ASM International, Metals Park, OH, 1992.
- [10] F. Chu, Private Communication, 1998.
- [11] E. Isaacson, H.B. Keller, *Analysis of Numerical Methods*, Dover, New York, 1994.
- [12] J.K. Lee, D.M. Barnett, H.I. Aaronson, *Metall. Trans. A* 8 (1977) 963–970.
- [13] P. Peralta, T.E. Mitchell, *Scripta Mater.* (1998), in preparation.
- [14] S.-Q. Xiao, S.A. Malloy, A.H. Heuer, U. Dahmen, *Phil. Mag. A* 72 (1995) 997–1013.
- [15] R.P. Goehner, J.R. Michael, *J. Res. Nat. Inst. Stand. Technol.* 101 (1996) 301–308.
- [16] A.P. Sutton, R.W. Balluffi, *Interfaces in Crystalline Materials*, Oxford University Press, New York, 1995.
- [17] K. Ito, H. Inui, Y. Shirai, M. Yamaguchi, *Phil. Mag. A* 72 (1995) 1075–1097.